^{11}C-ER176, a Radioligand for 18-kDa Translocator Protein, Has Adequate Sensitivity to Robustly Image All Three Affinity Genotypes in Human Brain

Masamichi Ikawa*[1], Talakad G. Lohith*[1], Stal Shrestha[1], Sanjay Telu[1], Sami S. Zoghbi[1], Sabrina Castellano[2], Sabrina Taliani[3], Federico Da Settimo[3], Masahiro Fujita[1], Victor W. Pike[1], and Robert B. Innis[1], the Biomarkers Consortium Radioligand Project Team

[1]Molecular Imaging Branch, National Institute of Mental Health, National Institutes of Health, Bethesda, Maryland; [2]Department of Medicine and Surgery, University of Salerno, Fisciano, Italy; and [3]Department of Pharmacy, University of Pisa, Pisa, Italy

For PET imaging of 18-kDa translocator protein (TSPO), a biomarker of neuroinflammation, most second-generation radioligands are sensitive to the single nucleotide polymorphism rs6971; however, this is probably not the case for the prototypical agent ^{11}C-PK11195 (^{11}C-labeled N-butan-2-yl-1-(2-chlorophenyl)-N-methylisoquinoline-3-carboxamide), which has a relatively lower signal-to-noise ratio. We recently found that ^{11}C-ER176 (^{11}C-(R)-N-sec-butyl-4-(2-chlorophenyl)-N-methylquinazoline-2-carboxamide), a new analog of ^{11}C-(R)-PK11195, showed little sensitivity to rs6971 when tested in vitro and had high specific binding in monkey brain. This study sought, first, to determine whether the sensitivity of ^{11}C-ER176 in humans is similar to the low sensitivity measured in vitro and, second, to measure the nondisplaceable binding potential (BP_{ND}, or the ratio of specific-to-nondisplaceable uptake) of ^{11}C-ER176 in human brain. **Methods:** Nine healthy volunteers—3 high-affinity binders (HABs), 3 mixed-affinity binders (MABs), and 3 low-affinity binders (LABs)—were studied with whole-body ^{11}C-ER176 PET imaging. SUVs from 60 to 120 min after injection derived from each organ were compared between genotypes. Eight separate healthy volunteers—3 HABs, 3 MABs, and 2 LABs—underwent brain PET imaging. The 3 HABs underwent a repeated brain scan after TSPO blockade with XBD173 (N-benzyl-N-ethyl-2-(7-methyl-8-oxo-2-phenylpurin-9-yl)acetamide) to determine nondisplaceable distribution volume (V_{ND}) via Lassen occupancy plotting and thereby estimate BP_{ND} in brain. **Results:** Regional SUV averaged from 60 to 120 min after injection in brain and peripheral organs with high TSPO densities such as lung and spleen were greater in HABs than in LABs. On the basis of V_{ND} determined via the occupancy plot, the whole-brain BP_{ND} for LABs was estimated to be 1.4 ± 0.8, which was much lower than that for HABs (4.2 ± 1.3) but about the same as that for HABs with ^{11}C-PBR28 ([methyl-^{11}C]N-acetyl-N-(2-methoxybenzyl)-2-phenoxy-5-pyridinamine)) (~1.2). **Conclusion:** Obvious in vivo sensitivity to rs6971 was observed in ^{11}C-ER176 that had not been expected from in vitro studies, suggesting that the future development of any improved radioligand for TSPO should consider the possibility that in vitro properties will not be reflected in vivo. We also found that ^{11}C-ER176 has adequately high BP_{ND} for all rs6971 genotypes. Thus, the new radioligand would likely have greater sensitivity in detecting abnormalities in patients.

The 18-kDa translocator protein (TSPO) is a mitochondrial protein that is highly expressed in phagocytic inflammatory cells, including activated microglia in the brain and macrophages in the periphery (1). As a result, numerous radioligands for PET that target TSPO have been developed to detect and quantify inflammation in the brain (2). The prototypical radioligand ^{11}C-labeled N-butan-2-yl-1-(2-chlorophenyl)-N-methylisoquinoline-3-carboxamide (^{11}C-PK11195) and its more active enantiomer ^{11}C-(R)-PK11195 have been used for in vivo imaging of TSPO for more than 2 decades (3). However, these radioligands have a relatively low signal-to-noise ratio. For example, the ratio of specific to nonspecific binding of ^{11}C-(R)-PK11195 in human brain was reported to be only about 0.2–0.5 (4,5). In contrast, some second-generation radioligands for TSPO, such as [methyl-^{11}C]N-acetyl-N-(2-methoxybenzyl)-2-phenoxy-5-pyridinamine) (^{11}C-PBR28), have a higher in vivo specific signal to TSPO than ^{11}C-(R)-PK11195. Owen et al. reported that the ratio of specific to nondisplaceable binding of ^{11}C-PBR28 in human brain was about 1.2 (6). In exchange for this improved specific signal to TSPO, most second-generation radioligands have varying degrees of sensitivity to the single nucleotide polymorphism rs6971 in the *TSPO* gene (7–9). This sensitivity has been problematic because some individuals (e.g., low-affinity binders [LABs] for ^{11}C-PBR28) must be excluded from analyses because the brain has too little uptake to quantify; commensurately, the remaining subjects must be corrected for being either high-affinity binders (HABs) or mixed-affinity binders (MABs).

Because brain uptake of the prototypical agent ^{11}C-(R)-PK11195 is insensitive to rs6971 (7), we evaluated analogs of PK11195 that were not sensitive in vitro but also had high specific (i.e., displaceable) binding in monkey brain. Among numerous candidates, ^{11}C-(R)-N-sec-butyl-4-(2-chlorophenyl)-N-methylquinazoline-2-carboxamide (^{11}C-ER176), a new quinazoline analog of ^{11}C-(R)-PK11195, was particularly promising. This ligand showed little in vitro sensitivity to rs6971. That is, its ratio of binding affinity in HABs to that in LABs was only 1.3 to 1 for ER176, whereas the comparable ratio

was 55 to 1 for PBR28 (Fig. 1) (9,10). It also performed well as a PET radioligand for TSPO in monkey brain, showing more than 80% specific (i.e., displaceable) binding (10).

Another complicating factor for TSPO radioligands is that genotype sensitivity may vary depending on the organ where it is expressed. For example, we found that ^{11}C-(R)-PK11195 showed no measurable sensitivity in the brain but clear sensitivity in several peripheral organs, including heart, lung, spleen, and kidney (7).

This study sought to determine the in vivo sensitivity of ^{11}C-ER176 in brain and peripheral organs in human subjects. For this purpose, we performed whole-body imaging for 9 subjects (3 subjects from each of the 3 genotypes: HAB, MAB, and LAB). In addition, to evaluate the ability of ^{11}C-ER176 to quantify TSPO density in the human brain, we performed brain imaging for 3 additional HABs at baseline and after blockade with N-benzyl-N-ethyl-2-(7-methyl-8-oxo-2-phenylpurin-9-yl)acetamide (XBD173), an agonist at the TSPO site (6,11), as well as an additional 3 MABs and 2 LABs at baseline; in that experiment, we measured nondisplaceable binding potential (BP_{ND}, the ratio of specific to nondisplaceable uptake) for human brain.

MATERIALS AND METHODS

Radiopharmaceutical Preparation

^{11}C-ER176 was prepared as described previously (10,12) with a specific activity of 121 ± 64 GBq/μmol at the time of injection (n = 20 batches) under our Investigational New Drug Application 122,236, which is available at https://kidbdev.med.unc.edu/databases/snidd/.

Subjects

Nine healthy volunteers participated in the whole-body PET scans (1 man and 2 women each with HAB, MAB, and LAB status; mean age ± SD, 30 ± 10 y). Eight separate healthy volunteers with either HAB, MAB, or LAB status participated in the brain PET scans (1 man and 2 women each for HAB and MAB status and 2 men with LAB status; 32 ± 9 y old). TSPO affinity type was determined by in vitro receptor binding to TSPO on leukocyte membranes or genetic analysis as previously described (8,13). The 3 HABs who participated in the brain PET scans received an oral dose of 90 mg of XBD173 as a partial blockade about 1.75 h before the second injection of ^{11}C-ER176 (6).

This study was approved by the Combined Neurosciences Institutional Review Board of the National Institute of Mental Health. All subjects signed an informed consent form.

Measuring ^{11}C-ER176 in Plasma

To determine arterial input function for brain PET scans, blood samples (1.5 mL each) were drawn from the radial artery at 20-s intervals until 200 s, followed by 3- to 6-mL samples at 3.6, 4, 4.5, 6, 8, 10, 15, 20, 30, 40, 50, 60, 75, and 90 min. The concentration of parent radioligand was measured after separating plasma from whole blood, as previously described (14).

Plasma concentration of the parent compound and whole blood activity were fitted to a triexponential function with weighting to minimize the relative distances of the measured values from the fitted values (relative weighting) using PMOD, version 3.6 (PMOD Technologies Ltd.). The parent fraction was fitted to a sigmoid function with relative weighting. The plasma free fraction (f_P) was measured by ultrafiltration as previously described (15).

Scan Procedures

For both whole-body and brain scans, ^{11}C-ER176 was intravenously injected over 3 min instead of 1 min because some rodents that received 100-fold the human equivalent dose showed slight and transient ataxia. Whole-body scans were performed on an Advance tomograph (GE Healthcare) as previously described for ^{11}C-PBR28 (16).

Brain scans were performed on a High-Resolution Research Tomograph scanner (CTI) or an Advance tomograph. After a ^{68}Ge transmission scan for attenuation correction, ^{11}C-ER176 was injected followed by a dynamic 3-dimensional emission acquisition for 90 min in 27 frames. PET images were reconstructed with filtered backprojection.

Dosimetry Analysis

Time–activity curves were derived from volumes of interest for each source organ (i.e., brain, heart, lungs, liver, spleen, kidneys, and thyroid) delineated on the whole-body images using PMOD. Residence times were calculated directly using the "Residence Times" model implemented in PMOD. Absorbed radiation doses were calculated by entering the residence times for each source organ into OLINDA/EXM, version 1.1 (17), using the model for a 70-kg adult man.

Brain Image Processing and Kinetic Analysis

Image and kinetic analyses for brain PET images were performed using PMOD. All time frames of dynamic PET images were realigned for motion correction. After coregistering both PET images and the N30R83 template to a sagittal MR image of 1-mm contiguous slices obtained using a 3.0-T Achieva device (Philips Healthcare), the PET data were derived using PMOD from the following volumes of interest based on the coregistered template (18): frontal, occipital, parietal, temporal, medial temporal, and cingulate cortices; thalamus; striatum; putamen; cerebellum; brain stem; cortical gray matter; white matter; and whole brain.

Estimating Binding Values

For whole-body images, the measured radioactivity in each organ was converted to SUV. Regional SUV averaged from 60 to 120 min after injection ($SUV_{60-120 \text{ min}}$) was used to measure radioligand uptake in each organ. This period was used because it better reflects receptor binding than the early period, which is strongly affected by blood flow.

For brain images, total volume of distribution (V_T), an index of receptor density that equals the ratio at equilibrium of the concentration of radioligand in tissue to that in plasma, was calculated with 1- and unconstrained 2-tissue compartment models (2TCM and 1TCM, respectively) using
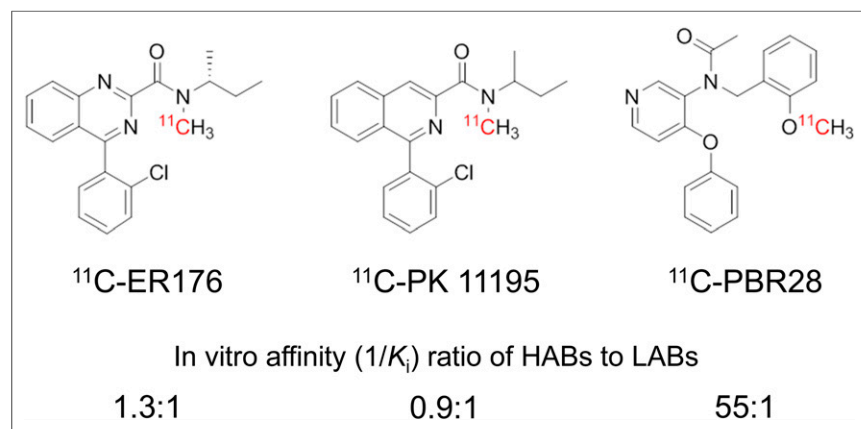

FIGURE 1. Chemical structures of 3 PET ligands for TSPO and in vitro affinity ratio of HABs to LABs in human brain tissue. Data are from previous publications (9,10).
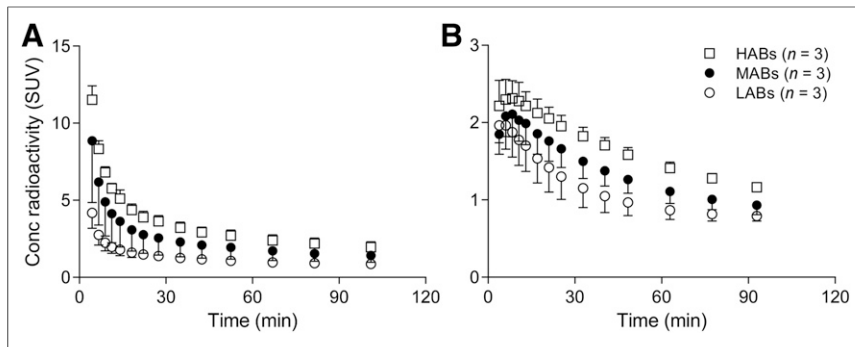
FIGURE 2. Time–activity curves for lung (A) and brain (B) after intravenous injection of ^{11}C-ER176 for each genotype. Error bars denote SD. Conc = concentration.

the radiometabolite-corrected plasma input function as previously described for ^{11}C-PBR28 (8). The concentration of radioligand in tissue represents the sum of specific binding (receptor-bound) and nondisplaceable uptake (nonspecifically bound and free radioligand in tissue water) (19).

To determine the minimal scan length for reliable measurements and also to indirectly assess whether ^{11}C-ER176 radiometabolites enter the brain, the time stability of V_T was examined by increasingly truncating the 90-min scan by 10-min increments to the shortest length of 0–50 min.

Estimating Nondisplaceable Distribution Volume (V_{ND})

A modification of the Lassen plot was used to estimate V_{ND} of ^{11}C-ER176 in brain in 2 ways: with an occupancy plot using the difference in V_T at baseline and after partial blockade with XBD173 in HABs, and with a polymorphism plot using the difference in V_T between 2 genetic groups (i.e., between HABs and MABs, between HABs and LABs, and between MABs and LABs) (6,20,21).

Statistical Analysis

Differences in SUV$_{60–120 min}$ for each organ were compared between genotypes by Kruskal–Wallis testing. The optimal compartment model (i.e., 1TCM vs. 2TCM) was chosen on the basis of the Akaike information criterion, model selection criterion, and F test (22). Regression analysis for the Lassen plot was performed using Pearson rank correlation. A P value of less than 0.05 was considered significant. All statistical analyses were performed with SPSS, version 22.0 (SPSS Inc.). Group data are expressed as mean ± SD.

TABLE 1
Organ Uptake of ^{11}C-ER176 for Each Genotype

	Organ uptake			
Organ	HABs ($n = 3$)	MABs ($n = 3$)	LABs ($n = 3$)	P
Brain	1.3 ± 0.1	1.0 ± 0.1	0.8 ± 0.1	0.05
Thyroid	2.8 ± 1.2	1.4 ± 0.4	1.3 ± 0.2	0.11
Lung	2.2 ± 0.3	1.5 ± 0.5	0.9 ± 0.1	0.06
Heart	6.8 ± 0.3	5.0 ± 0.6	3.5 ± 0.9	0.04
Liver	3.0 ± 0.7	3.3 ± 0.3	2.8 ± 0.1	0.25
Spleen	4.3 ± 0.1	3.7 ± 0.8	2.7 ± 0.3	0.06
Kidney	3.9 ± 0.4	3.6 ± 0.3	2.5 ± 0.2	0.10

Data are mean SUV$_{60–120 min}$ ± SD. P values were derived from Kruskal–Wallis test between genotypes.

RESULTS

Pharmacologic Effects

No adverse or clinically detectable pharmacologic effects were observed with ^{11}C-ER176 for any of the 17 subjects or in any of the 3 subjects who also received XBD173. Supplemental Table 1 shows the administered doses (supplemental materials are available at http://jnm.snmjournals.org). No significant changes in vital signs or electrocardiograms were observed during the PET scan or in the results of laboratory tests repeated after the scan.

Whole-Body Biodistribution and Dosimetry Estimates

Whole-body imaging clearly showed that the in vivo binding of ^{11}C-ER176 was sensitive to rs6971. Uptake for brain and lung was lower in LABs than in HABs at all time points, with intermediate values for MABs (Fig. 2). SUV$_{60–120 min}$ showed a significant difference between genotypes in heart ($P < 0.05$). The same tendency was observed in brain, lung, and spleen (Table 1).

The residence time of organs was calculated for the 9 subjects (Supplemental Table 2). The effective dose was 4.1 ± 0.4 μSv/MBq (Supplemental Table 3), which is similar to that of other ^{11}C-labeled radioligands (23).

Kinetic Analysis

Kinetic analysis of brain and plasma data obtained 3 major results. First, brain time–activity curves fitted better with 2TCM than 1TCM. The unconstrained 2TCM fitting converged in brain time–activity curves from all regions, in all scans, and in all genotypes, both at baseline and after blockade with XBD173 in HABs (Fig. 3A). Compared with the 1TCM, the 2TCM showed lower mean Akaike information criterion scores (130 vs. 242) and higher mean model selection criterion scores (6.4 vs. 2.9). An F test also showed that the goodness of fit was significantly better with the 2TCM than with the 1TCM in all 154 fittings over a total of 11 scans, indicating the presence of significant amounts of both specific and nonspecific binding in human brain. The 2TCM identified V_T well, with an average SE of 2.4% across brain regions. Regional V_T values (mL·cm^{-3}) were consistent with the known distribution of TSPO, showing high levels in the brain stem (4.3) and low levels in the putamen (3.2) at baseline for HABs (Table 2).

With regard to the second result, V_T values were stable from 60 to 90 min and were well identified (SE < 10%) in all 3 genotypes with the exception of 1 MAB and in the 3 HABs after blockade, which had low specific binding like that in LABs (Fig. 4), indicating negligible accumulation of radiometabolites regardless of the genotype.

The third major finding was that V_T values were higher for HABs than for LABs in all regions of interest, with intermediate values for MABs (Table 2). The whole-brain V_T in HABs (3.3 ± 0.9 mL·cm^{-3}) was about 1.2-fold higher than that in MABs (2.9 ± 0.9 mL·cm^{-3}) and about 2.2-fold higher than that in LABs (1.6 ± 0.5 mL·cm^{-3}).

Estimating Specific and Nondisplaceable Binding

We attempted to estimate BP_{ND} in 2 ways: by receptor blockade in HABs and by the so-called polymorphism plot, which compares uptake in genetic groups (6,20,21). After receiving XBD173, all 3 HABs showed marked blocking effects, both in brain and in plasma. That is, receptor blockade decreased peak uptake in brain,
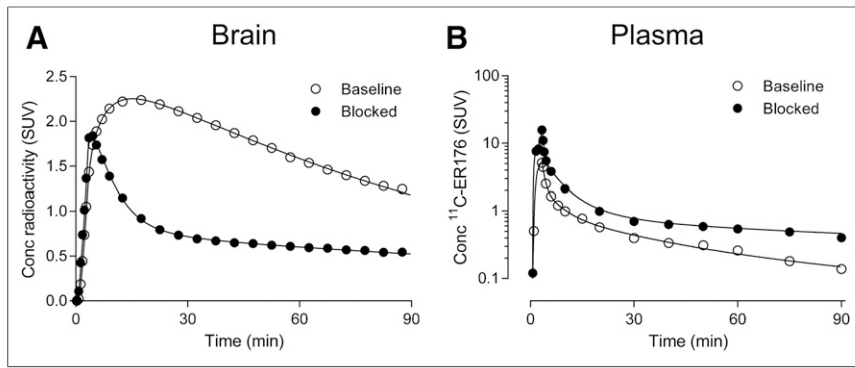
FIGURE 3. Brain uptake and plasma radioactivity concentrations (conc) of ^{11}C-ER176 in representative HAB at baseline (○) and after blockade with 90 mg of XBD173 (●). (A) Brain time–activity curves from gray matter with unconstrained 2TCM fitting. (B) Time courses of parent concentration in arterial plasma fitted by multiplying triexponential-fitted total plasma radioactivity and sigmoid-fitted plasma parent fraction.

increased washout, and decreased total uptake over the 90-min scan (Fig. 3A). In plasma, XBD173 significantly increased the concentration of ^{11}C-ER176, consistent with its blocking the distribution of the radioligand to organs of the body (Fig. 3B) (7). The Lassen plot of baseline and blocked scans in individual subjects showed an excellent linear correlation and had a mean V_{ND} of 0.65 ± 0.01 mL·cm^{-3} and receptor occupancy (i.e., slope) of $90\% \pm 13\%$ (Fig. 5A). Based on the estimated V_{ND} (0.65), the BP_{ND} for whole brain was 4.2 ± 1.3 in HABs, 3.4 ± 1.4 in MABs, and 1.4 ± 0.8 in LABs. The BP_{ND} ratios, which are equivalent to the ratio of specific binding, were 1.2 in HABs/MABs and 3.0 in HABs/LABs.

In addition to blocking the distribution of ^{11}C-ER176 to organs, XBD173 also decreased radioligand binding to plasma proteins, presumably by blocking TSPO in white blood cells. That is, XBD173 increased the f_P of ^{11}C-ER176 in all 3 HABs by about 20%, from $3.3\% \pm 0.7\%$ to $4.1\% \pm 0.7\%$. Because only free drug can cross the blood–brain barrier, we corrected the Lassen plot for each individual's value of f_P at baseline and after XBD173. This gave an estimate of 15.5 ± 2.0 mL·cm^{-3} for a mean V_{ND} corrected for f_P (V_{ND}/f_P), with minimal effect on receptor occupancy ($92\% \pm 10\%$) (Fig. 5B). Compared with the Lassen analysis noted above, correction for f_P increased whole-brain BP_{ND} for HABs by 31% (5.5 ± 1.1), for MABs by 19% (4.1 ± 1.6), and for LABs by

25% (1.8 ± 0.3). The ratios of BP_{ND} after correcting for f_P were 1.3 in HABs/MABs and 3.1 in HABs/LABs.

The polymorphism plot, which was the second method of estimating BP_{ND}, had a poor linear fit in the comparison between HABs and MABs and therefore provided questionable estimates of V_{ND} (Supplemental Fig. 1). The poor fitting was likely caused by the relatively small differences between HABs and MABs, which itself formed the y-axis. For example, the whole-brain V_T of MABs was only 16% less than that of HABs (Table 2).

DISCUSSION

Using a sample size of 2 or 3 subjects per genotype, we determined that ER176 is sensitive in vivo to the rs6971 polymorphism. This contrasts with its low sensitivity to rs6971 in vitro, as determined using homogenates of human brain and white blood cells (10), and highlights an additional challenge to the future development of improved radioligands for TSPO, as the in vitro properties used to screen candidates may not be reflected in vivo. The cause of the discrepant genetic sensitivity between in vitro and in vivo conditions is unknown but may involve in vivo protein–protein interactions that are disrupted by tissue homogenization and dilution of postmortem tissue or other in vitro conditions. Such discrepancies between in vitro and in vivo binding are well known for G-protein–coupled receptors, where attachment of the receptor to its G-protein increases the affinity of agonists (24). A similar interaction may occur for TSPO with any of the 3 proteins that combine with TSPO to form the so-called permeability transition pore (25,26). In addition, the higher specific binding of improved radioligands may increase in vivo sensitivity to the genotype, in contrast to the prototypical agent [11]C-(R)-PK11195 that has a relatively lower signal-to-noise ratio in brain and may lack the sensitivity needed to detect a genetic effect (4,5,7).

Our receptor blocking study using XBD173 found that ^{11}C-ER176 had adequately high BP_{ND} for all genotypes. The whole brain BP_{ND}—without correcting for f_P—was 4.2 ± 1.3 and 1.4 ± 0.8 for HABs and LABs, respectively; both of these values were

TABLE 2
V_T and V_T/f_P of ^{11}C-ER176 at Baseline for Each Genotype

| Brain region	V_T			V_T/f_P		
	HABs (n = 3)	MABs (n = 3)	LABs (n = 2)	HABs (n = 3)	MABs (n = 3)	LABs (n = 2)
Gray matter	3.5 ± 0.9	2.9 ± 1.0	1.6 ± 0.5	106.3 ± 17.0	78.9 ± 26.0	43.2 ± 5.5
Thalamus	4.1 ± 1.2	3.2 ± 0.9	1.8 ± 0.6	123.1 ± 23.8	87.3 ± 25.7	48.7 ± 6.3
Putamen	3.2 ± 0.9	2.9 ± 1.0	1.5 ± 0.5	97.4 ± 19.3	80.1 ± 27.0	40.7 ± 5.3
Cerebellum	3.5 ± 0.9	2.9 ± 0.8	1.6 ± 0.5	105.4 ± 12.8	80.0 ± 23.1	44.0 ± 5.4
Brain stem	4.3 ± 1.0	3.8 ± 1.0	1.9 ± 0.6	128.2 ± 16.3	103.8 ± 32.6	52.0 ± 5.2
Whole brain	3.3 ± 0.9	2.9 ± 0.9	1.6 ± 0.5	100.3 ± 16.8	79.0 ± 25.4	42.7 ± 4.8

Data are mean mL·cm^{-3} ± SD.
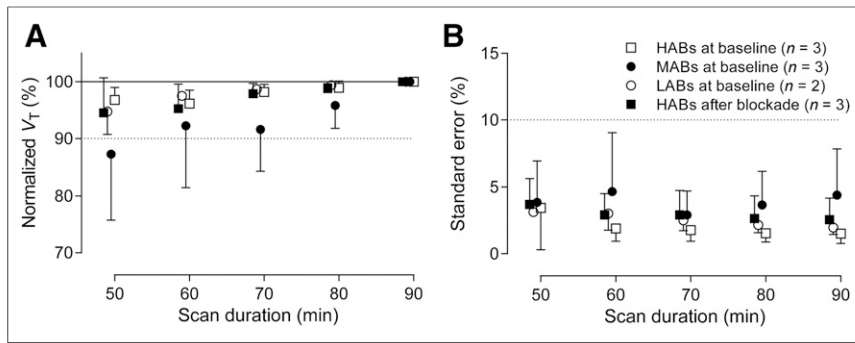
FIGURE 4. Time–stability analysis: V_T obtained from both baseline scans for each genotype and blocked scans for HABs, as well as its identifiability, is plotted as function of duration of image acquisition. (A) V_T was calculated for putamen using unconstrained 2TCM with increasingly truncated acquisition times. Values are normalized as percentage of terminal value attained from 90 min of imaging. (B) Corresponding percentage SE, which is inversely proportional to identifiability, is plotted. Data are mean ± SD.

higher than that reported for ^{11}C-PBR28 in HABs ($\sim$1.2) (6). Furthermore, V_T for ^{11}C-ER176 was well identified by the 2TCM in all genotypes. We also examined time stability under conditions of variable specific binding (i.e., HABs > MABs > LABs > blocked scans for HABs) and found that V_T was within 10% of the final value by 60–90 min in all but 1 MAB (Fig. 4). The high BP_{ND} and good identifiability in all genotypes, including LABs, suggests that this new radioligand would likely have better sensitivity in detecting abnormalities in patients and that LABs may not need to be excluded as they are for ^{11}C-PBR28.

Both the polymorphism and the Lassen occupancy plots examine the linear relationship between some measure of specific binding (y-axis) and V_T (x-axis) for multiple brain regions. For the polymorphism plot, specific binding is the difference in V_T between genetic groups; for the Lassen plot, specific binding is the difference between baseline and blocked conditions. For both plots, the linear extrapolation to the x-intercept provides the value of V_T in an imaginary region with no specific binding—namely, V_{ND}. The polymorphism plot for ^{11}C-ER176 was noisy and provided

questionable values for V_{ND} (Supplemental Fig.e 1). The noise derived in part from the relatively small difference in whole-brain V_T in HABs (3.3 ± 0.9 mL·cm^{-3}) compared with that in MABs (2.9 ± 0.9 mL·cm^{-3}). In contrast, the measure of specific binding for the Lassen plot was quite substantial, as V_T was 3.3 ± 0.9 mL·cm^{-3} at baseline and only 0.9 ± 0.2 mL·cm^{-3} after blockade.

But why was the V_T of MABs only slightly smaller than that of HABs? One possible reason is that TSPO exists mainly as a dimer in vivo, on the basis of its recently reported x-ray crystallographic structure (27). If it were only a monomer, MABs would be expected to have 2 types of TSPO: 50% HAB and 50% LAB. In reality, TSPO may exist in a quite complicated situation with a mixture of monomers, dimers, and higher-mers, implying that TSPO in MABs comprises roughly half heteromers (consisting of both HAB and LAB subunits) and half homomers of HAB or LAB subunits. Our study showed that the in vivo affinity of homozygous LAB subjects was much lower than that of HAB subjects, but we do not know the affinity of the heteromers of HAB and LAB subunits. In fact, the small difference in BP_{ND} between HAB and MAB subjects (ratio, 1.2) suggests that most of the heteromers maintain significant affinity for ^{11}C-ER176. For ^{11}C-PBR28, in contrast, the difference between BP_{ND} in HABs and MABs was substantial (ratio, 2.5) (6), suggesting that the heteromer has diminished affinity for this radioligand; this, in turn, allowed the polymorphism plot to be less noisy and to reliably estimate V_{ND}.

CONCLUSION

Our goal was to develop an improved TSPO radioligand that was insensitive to genotype, thereby allowing the imaging of LABs, but we were only partially successful; specifically, we found that ^{11}C-ER176 is sensitive to rs6971 in vivo but still allows quantitation in LABs. ^{11}C-ER176 provided a high BP_{ND} value equivalent to that of ^{11}C-PBR28 in HABs, which was stably identified within 60 min of imaging.
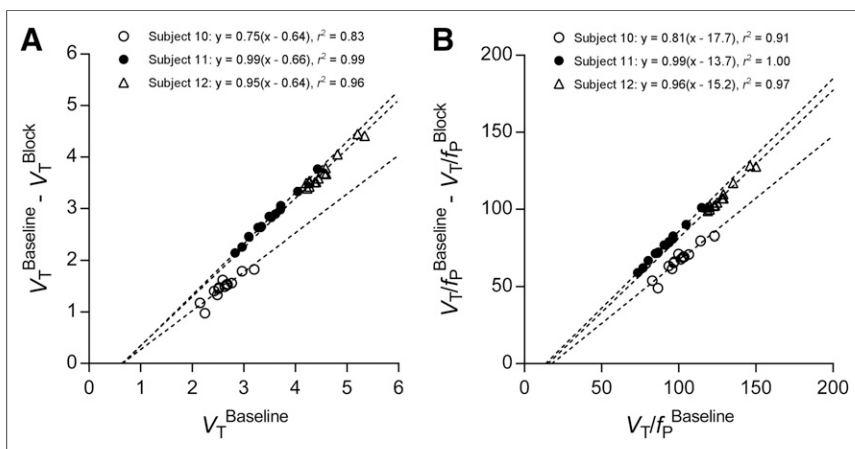
FIGURE 5. Lassen plot to determine V_{ND} (A) or V_{ND}/f_P (B) of ^{11}C-ER176 in brain of 3 HABs. Each point represents brain region in individual subject. Pearson r^2 is shown for each relationship. $P < 0.0001$ for all correlations. For these 3 subjects, V_{ND}, which corresponds to x-intercept, was 0.64, 0.66, and 0.64 mL·cm^{-3} and V_{ND}/f_P was 17.7, 13.7, and 15.2 mL·cm^{-3}.

REFERENCES

1. Papadopoulos V, Baraldi M, Guilarte TR, et al. Translocator protein (18kDa): new nomenclature for the peripheral-type benzodiazepine receptor based on its structure and molecular function. *Trends Pharmacol Sci.* 2006;27:402–409.
2. Cagnin A, Kassiou M, Meikle SR, Banati RB. Positron emission tomography imaging of neuroinflammation. *Neurotherapeutics.* 2007;4:443–452.
3. Venneti S, Lopresti BJ, Wiley CA. The peripheral benzodiazepine receptor (translocator protein 18kDa) in microglia: from pathology to imaging. *Prog Neurobiol.* 2006;80:308–322.
4. Kropholler MA, Boellaard R, Schuitemaker A, Folkersma H, van Berckel BN, Lammertsma AA. Evaluation of reference tissue models for the analysis of [^{11}C](*R*)-PK11195 studies. *J Cereb Blood Flow Metab.* 2006;26:1431–1441.
5. Turkheimer FE, Edison P, Pavese N, et al. Reference and target region modeling of [^{11}C]-(*R*)-PK11195 brain studies. *J Nucl Med.* 2007;48:158–167.
6. Owen DR, Guo Q, Kalk NJ, et al. Determination of [^{11}C]PBR28 binding potential in vivo: a first human TSPO blocking study. *J Cereb Blood Flow Metab.* 2014;34:989–994.
7. Kreisl WC, Fujita M, Fujimura Y, et al. Comparison of [^{11}C]-(*R*)-PK 11195 and [^{11}C]PBR28, two radioligands for translocator protein (18 kDa) in human and monkey: implications for positron emission tomographic imaging of this inflammation biomarker. *Neuroimage.* 2010;49:2924–2932.
8. Kreisl WC, Jenko KJ, Hines CS, et al. A genetic polymorphism for translocator protein 18 kDa affects both in vitro and in vivo radioligand binding in human brain to this putative biomarker of neuroinflammation. *J Cereb Blood Flow Metab.* 2013;33:53–58.
9. Owen DR, Howell OW, Tang SP, et al. Two binding sites for [^{3}H]PBR28 in human brain: implications for TSPO PET imaging of neuroinflammation. *J Cereb Blood Flow Metab.* 2010;30:1608–1618.
10. Zanotti-Fregonara P, Zhang Y, Jenko KJ, et al. Synthesis and evaluation of translocator 18 kDa protein (TSPO) positron emission tomography (PET) radioligands with low binding sensitivity to human single nucleotide polymorphism rs6971. *ACS Chem Neurosci.* 2014;5:963–971.
11. Rupprecht R, Rammes G, Eser D, et al. Translocator protein (18 kD) as target for anxiolytics without benzodiazepine-like side effects. *Science.* 2009;325:490–493.
12. Castellano S, Taliani S, Milite C, et al. Synthesis and biological evaluation of 4-phenylquinazoline-2-carboxamides designed as a novel class of potent ligands of the translocator protein. *J Med Chem.* 2012;55:4506–4510.
13. Kreisl WC, Lyoo CH, McGwier M, et al. In vivo radioligand binding to translocator protein correlates with severity of Alzheimer's disease. *Brain.* 2013;136:2228–2238.
14. Zoghbi SS, Shetty HU, Ichise M, et al. PET imaging of the dopamine transporter with ^{18}F-FECNT: a polar radiometabolite confounds brain radioligand measurements. *J Nucl Med.* 2006;47:520–527.
15. Gandelman MS, Baldwin RM, Zoghbi SS, Zea-Ponce Y, Innis RB. Evaluation of ultrafiltration for the free-fraction determination of single photon emission computed tomography (SPECT) radiotracers: beta-CIT, IBF, and iomazenil. *J Pharm Sci.* 1994;83:1014–1019.
16. Brown AK, Fujita M, Fujimura Y, et al. Radiation dosimetry and biodistribution in monkey and man of ^{11}C-PBR28: a PET radioligand to image inflammation. *J Nucl Med.* 2007;48:2072–2079.
17. Stabin MG, Sparks RB, Crowe E. OLINDA/EXM: the second-generation personal computer software for internal dose assessment in nuclear medicine. *J Nucl Med.* 2005;46:1023–1027.
18. Hammers A, Allom R, Koepp MJ, et al. Three-dimensional maximum probability atlas of the human brain, with particular reference to the temporal lobe. *Hum Brain Mapp.* 2003;19:224–247.
19. Innis RB, Cunningham VJ, Delforge J, et al. Consensus nomenclature for in vivo imaging of reversibly binding radioligands. *J Cereb Blood Flow Metab.* 2007;27:1533–1539.
20. Cunningham VJ, Rabiner EA, Slifstein M, Laruelle M, Gunn RN. Measuring drug occupancy in the absence of a reference region: the Lassen plot re-visited. *J Cereb Blood Flow Metab.* 2010;30:46–50.
21. Guo Q, Colasanti A, Owen DR, et al. Quantification of the specific translocator protein signal of ^{18}F-PBR111 in healthy humans: a genetic polymorphism effect on in vivo binding. *J Nucl Med.* 2013;54:1915–1923.
22. Fujita M, Seibyl JP, Verhoeff NP, et al. Kinetic and equilibrium analyses of [^{123}I]epidepride binding to striatal and extrastriatal dopamine D_2 receptors. *Synapse.* 1999;34:290–304.
23. Zanotti-Fregonara P, Innis RB. Suggested pathway to assess radiation safety of ^{11}C-labeled PET tracers for first-in-human studies. *Eur J Nucl Med Mol Imaging.* 2012;39:544–547.
24. Thompson MD, Cole DE, Jose PA, Chidiac P. G protein-coupled receptor accessory proteins and signaling: pharmacogenomic insights. *Methods Mol Biol.* 2014;1175:121–152.
25. Azarashvili T, Grachev D, Krestinina O, et al. The peripheral-type benzodiazepine receptor is involved in control of Ca^{2+}-induced permeability transition pore opening in rat brain mitochondria. *Cell Calcium.* 2007;42:27–39.
26. Rone MB, Fan J, Papadopoulos V. Cholesterol transport in steroid biosynthesis: role of protein-protein interactions and implications in disease states. *Biochim Biophys Acta.* 2009;1791:646–658.
27. Li F, Liu J, Zheng Y, Garavito RM, Ferguson-Miller S. Protein structure: crystal structures of translocator protein (TSPO) and mutant mimic of a human polymorphism. *Science.* 2015;347:555–558.